Supporting Information

Accelerated Electrocatalyst Degradation Testing by Accurate and Robust Forecasting of Multidimensional Kinetic Model with Bayesian Data Assimilation

Miao Wang,[a] Akimitsu Ishii,[b] and Ken Sakaushi[a,]*

[a]*Research Center for Energy and Environmental Materials, National Institute for Materials Science, 1-1 Namiki, Tsukuba, Ibaraki 305-0044, Japan*

[b]*International Center for Young Scientists, National Institute for Materials Science, 1-2-1 Sengen, Tsukuba, Ibaraki 305-0047, Japan*

**Email: SAKAUSHI.Ken@nims.go.jp*

Part 1. OER degradation model

For the microkinetic OER, we could use a steady-state approximation to give a full description based on the widely used adsorption evolution mechanism, as shown below (here we exemplify H_2O as the reactant).

$$* + H_2O \leftrightarrow *OH + H^+ + e^- \quad (1)$$

$$*OH \leftrightarrow *O + H^+ + e^- \quad (2)$$

$$*O + H_2O \leftrightarrow *OOH + H^+ + e^- \quad (3)$$

$$*OOH \leftrightarrow * + O_2 + H^+ + e^- \quad (4)$$

in which * represents the active site.

According to the steady-state approximation and transition-state theory, the rate coefficient (k_{ij}, which herein merges activity terms of other reactants for simplification) in the elementary step from the i^{th} to j^{th} intermediate and surface coverages of the i^{th} intermediate (θ_i) follow:

$$\sum_j (k_{ji}\theta_j - k_{ij}\theta_i) = 0 \quad \text{(eq. S1)}$$

$$k_{ij} = A_{ij} e^{-\frac{\triangle G_{ij}^{\neq}}{RT}} \quad \text{(eq. S2)}$$

$$A_{ij} = \kappa \frac{k_B T}{h} [X_{ij}] \quad \text{(eq. S3)}$$

in which A_{ij} is the coefficient including the activity of reactant $[X_{ij}]$, $\triangle G_{ij}^{\neq}$ is the free energy of activation in each electron-transfer step (from the i^{th} intermediate to the j^{th} intermediate), T is reaction temperature, κ is transmission coefficient (commonly equals unity), k_B is Boltzmann constant, h is Planck constant.

For the surface coverages, we have:

$$\theta_1 + \theta_2 + \theta_3 + \theta_4 = 1 \quad \text{(eq. S4)}$$

The reaction rate r can be obtained:

$$r = k_{12}\theta_1 - k_{21}\theta_2 = k_{23}\theta_2 - k_{32}\theta_3 = k_{34}\theta_3 - k_{43}\theta_4 = k_{41}\theta_4 - k_{14}\theta_1 \quad \text{(eq. S5)}$$

By solving the above equations, we have:

$$r = (k_{12}k_{23}k_{34}k_{41} - k_{14}k_{43}k_{32}k_{21}) / [(k_{23}k_{34}k_{41} + k_{21}k_{34}k_{41} + k_{21}k_{32}k_{41} + k_{21}k_{32}k_{43}) + (k_{14}k_{43}k_{32} + k_{34}k_{41}k_{12} + k_{32}k_{41}k_{12} + k_{12}k_{43}k_{32}) + (k_{23}k_{14}k_{43} + k_{21}k_{14}k_{43} + k_{41}k_{12}k_{23} + k_{43}k_{12}k_{23}) + (k_{14}k_{23}k_{34} + k_{34}k_{21}k_{14} + k_{32}k_{21}k_{14} + k_{12}k_{23}k_{34})] \quad \text{(eq. S6)}$$

The OER current (I) can be further calculated through:

$$I = 4FC_{site}r \quad \text{(eq. S7)}$$

where F is the Faraday constant, C_{site} is the number of active sites.

However, the above microkinetic description for OER is too complicated to resolve all the parameters effectively. Thus, we have to seek a simpler and still general alternative. The energetic span model (**Scheme S1** below) was derived similar to the above microkinetic analysis (of course, it was for thermocatalysis but not electrocatalysis in the beginning), including every free energy of activation in each step. [1-6] The initial full microkinetic analysis-based model could be finally simplified to a concise formation analogous to Butler-Volmer framework, by using the maximum term of energy, *i.e.*, the energetic span. Therefore, the energetic span model used in our work is a simplified and convenient description for OER based on a full microkinetic framework.

Through the above simple model, we further derived the degradation model (as discussed below) and combined it with data assimilation method to make reliable lifetime forecasting for the OER degradation. Even though this energetic span model-derived degradation model only provided apparent kinetic parameters, it was successfully applied to quantifying OER degradation under various conditions (*e.g.*, pH from acid to alkali, different temperatures, various materials, as shown in **Figure 2c,2d** in main text and **Figure S6**, **Figure S7**), demonstrating its promising universality for future practical applications.

To further grasp the degradation process in a real microkinetic scale, apart from the demanding for a more comprehensive dissolution model after the model diagnosis (**Figure S11**), a higher-level-ladder description of the OER process is expected to understand the structure evolution of electrode-electrolyte interface during degradation as well as the resultant effects. This level-up OER model may include thermodynamics, microkinetics, mass transport effect, electric double layer effect, and even the reconstruction of catalyst during the reaction.[7, 8] However, the above points are still challenging at present and more endeavours will be conducted in our future work.

Even though energetic span model is convenient, its assumption may not meet some situations. From a microscopic viewpoint, surface configurations on electrocatalyst are usually various in a practical reaction system, such as different coordinated metal sites, non-metal ligands, and defects. These diverse local structures result in various adsorption energies for the reaction intermediates, even a near-continuum distribution of adsorption energies.[9] The active sites with

various properties in an atomic resolution can be described by kinetic Monte-Carlo (KMC) methods.[10] However, KMC methods require large computational resources and additional expert knowledge of statistical mechanics. The high complexity makes KMC methods challenging to be used in our work to resolve key parameters for an effective lifetime forecast toward OER performance degradation.

Considering the above issues, in this work we focused on the typical RuO_x materials usually used as benchmark in many studies. We discussed the OER process based on a mean-field model and the widely applied adsorption evolution mechanism (can be regarded as "first-order" elementary steps mathematically), to avoid too complicated analyses and suit the application of the energetic span model. In addition, the site coverage matches the energetic span model, as the "catalytic intermediates" used in deriving the model is identical to including the coverage term mathematically.[3]

Therefore, given the practical applicability for our degradation model, in this work we finally used the energetic span model, *i.e.*, a simple equation as eq. S8, to implicitly include a microkinetic framework for the OER.

According to the energetic span model, the turnover frequency (TOF) for OER could be written as: [1-6]

$$TOF = k_{00}e^{-\frac{\delta G}{RT}} \quad \text{(eq. S8)}$$

where k_{00} is the pre-exponential factor for OER, R is gas constant, T is the temperature, δG is the energetic span.

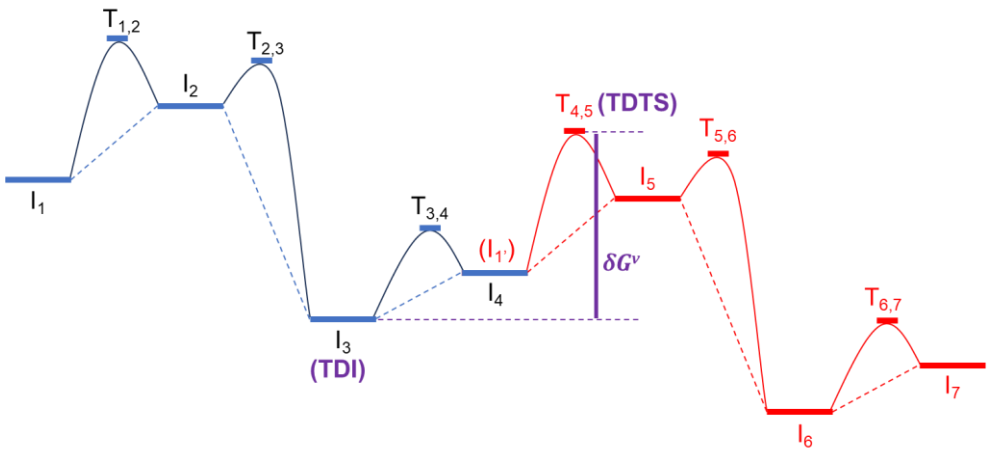

Scheme S1. The approach to determine the energetic span (δG): $\delta G = \max\{T_{i,i+1} - I_j, i > j\}$, where $T_{i,i+1}$ is the free energy of the transition state between the i^{th} and $(i+1)^{th}$ intermediate states (I_i and I_{i+1}). The TOF-determining intermediate (TDI) is the intermediate state that determines δG, while the TOF-determining transition state (TDTS) is the transition state $T_{i,i+1}$ that determines δG, so that we also have $\delta G = TDTS - TDI$, as shown in the scheme. For more details, please refer to the previous publications.[1-6]

For the above energetic span δG, we conducted a first-order approximation of the Taylor polynomial relating to the potential E at a fixed potential E_0:[11]

$$\delta G \approx \delta G(E_0) + \frac{\partial \delta G}{\partial E}|_{E_0}(E - E_0) \quad \text{(eq. S9)}$$

So that the TOF could be expressed as:

$$TOF \approx k_{00}e^{-\frac{\delta G(E_0)+\frac{\partial \delta G}{\partial E}|_{E_0}(E-E_0)}{RT}} \quad \text{(eq. S10)}$$

which was further simplified as:

$$TOF = k'_{00}\, e^{\alpha E} \quad \text{(eq. S11-1)}$$

$$k'_{00} = k_{00} e^{-\frac{\delta G(E_0) - \frac{\partial \delta G}{\partial E}|_{E_0}(E_0)}{RT}} \quad \text{(eq. S11-2)}$$

$$\alpha = -\frac{\frac{\partial \delta G}{\partial E}|_{E_0}}{RT} \quad \text{(eq. S11-3)}$$

Given that the production of one oxygen molecule took four electrons, the OER current I could be written by considering the time-dependent number of active site $S(t)$ and the current from the substrate c:

$$I = 4FS(t)\,TOF + c = 4FS(t)k'_{00}\,e^{\alpha E} + c \quad \text{(eq. S12)}$$

which was simplified as:

$$I = k_0 S(t)\,e^{\alpha E} + c \quad \text{(eq. S13-1)}$$

$$k_0 = 4Fk'_{00} \quad \text{(eq. S13-2)}$$

Practically, the potential E was:

$$E = E_{app} - IR_u \quad \text{(eq. S14)}$$

where E_{app} is the applied potential with respect to the reference electrode, R_u is the resistance including the solution resistance and the working electrode resistance (mainly by the substrate). We used a first-order approximation to describe the time-dependent R_u:

$$R_u(t) \approx R_0 + r_{RWE,1}t \quad \text{(eq. S15)}$$

where R_0 is the resistance in the initial, $r_{RWE,1}$ is the rate of resistance change due to the substrate passivation, t is time.

Combing eq. S13-eq. S15, we got the applied potential-time-current relationship to quantify the OER degradation process:

$$E_{app} = \frac{1}{\alpha} ln \frac{I-c}{k_0 S(t)} + I(R_0 + r_{RWE,1}t) \quad \text{(eq. S16)}$$

We focused on the time-dependent active site number $S(t)$ by dissolution.[12] This anodic dissolution phenomenon could be understood by Pourbaix diagram from a thermodynamic viewpoint: at an anodic potential soluble species were formed due to the catalyst reconstruction.[13] We used a semi-empirical description analogous to the law of mass action by considering the dissolution of the electrocatalyst during OER, which was crucial for the electrocatalyst degradation:[14]

$$r = k^{dis} S(t)^x \quad \text{(eq. S17)}$$

$$k^{dis} = k_0^{dis} e^{\alpha^{dis}(E_{app} - IR_u)} \quad \text{(eq. S18)}$$

$$\frac{dS(t)}{dt} = -r \quad \text{(eq. S19)}$$

$$S(0) = S_{max} \quad \text{(eq. S20)}$$

where r is the rate of dissolution, k^{dis} is the dissolution coefficient, k_0^{dis} is the pre-exponential factor for dissolution, α^{dis} is the coefficient for the influence of potential on dissolution, x is the reaction order for the dissolution, $S(0)$ is the number of active site in the initial (here we denoted it as S_{max}). Combining eq. S16-eq. S20, $S(t)$ could be finally derived as:

$$S(t) = \left(\left(k't + \frac{{S_{max}}^{1-x'}}{-1+x'}\right)(-1+x')\right)^{\frac{1}{1-x'}} \quad \text{(eq. S21)}$$

$$k' = k_0^{dis}\,(\frac{I-c}{k_0})^{\frac{\alpha^{dis}}{\alpha}} \quad \text{(eq. S22)}$$

$$x' = x - \frac{\alpha^{dis}}{\alpha} \quad \text{(eq. S23)}$$

In summary, the OER electrocatalyst degradation could be quantitatively described by the combination of eq. S16 and eq. S21.

For the degradation mechanisms, we first summarized various possible processes: 1) dissolution of catalyst, 2) agglomeration, 3) detachment of catalyst, 4) blocking effect by adsorption/(re)deposition, 5) bubble blocking, 6) passivation and 7) dissolution of substrate. Nonetheless, we paid attention to the significantly noticeable factor in most case, *i.e*, the catalyst dissolution.

To make it more reliable, we elaborately designed the whole experiments to minimize the influences caused by other degradation processes: 1) using fierce stirring to promote the desorption of oxygen bubbles (as the typical experimental configuration in **Figure S3**); 2) loading RuO_x on the substrate by pyrolyzing rather than mixing RuO_x powders with binder (such as Nafion), to avoid agglomeration and detachment of catalyst during OER testing as possible; 3) adopting non-membrane configuration and fierce stirring to facilitate the deposition of dissolved Ru species on counter electrode to minimize the adsorption/(re)deposition blocking effect; 4) using the highly corrosion-resistant titanium/titanium oxide as the substrate to avoid the dissolution of substrate during OER. As for the passivation of substrate, we included this process in our degradation model, as discussed above. However, in our practical measurements of this work, this substrate passivation effect could be almost ignored, as discussed in **Table S2**.

Therefore, we mainly ascribed the degradation during OER to the catalyst dissolution. This was further verified by the obvious disappearance of the catalyst layer after the degradation testing (**Figure S1**), as well as the decreased amount of Ru by inductively coupled plasma-optical emission spectrometry (ICP-OES) (before testing: 0.135 mg cm^{-2}, after testing in 1 M KPi: 0.06 mg cm^{-2}). Such a simplification of the degradation process benefited the availability of resolving parameters with appropriate amount (four parameters) in our degradation model, *i.e.*, the coefficient for the influence of potential on the intrinsic OER activity α, the pre-exponential factor for OER k_0, the apparent dissolution coefficient (in this work termed dissolution factor) k', and the apparent reaction order for dissolution x', as shown in the model equations above.

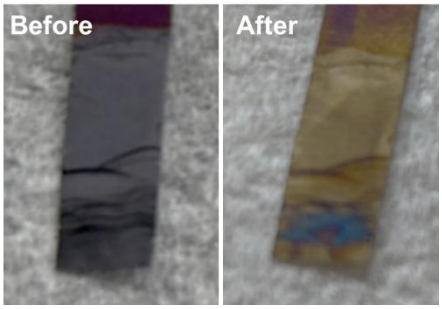

Figure S1. The RuO_x loaded on Ti substrate was obviously dissolved after the degradation testing in 0.1 M H_2SO_4 (300 mA cm^{-2}, 35 °C).

As for the model, we further underlined the importance of adopting a simplified model proposed in our work. The discussion is shown below.

As summarized in the main text, the loss of active site could be accurately described as following:

$$\frac{dS(t)}{dt} = f_{dis}(t) + f_{agg}(t) + f_{detach}(t) + f_{ad-dep}(t) + f_{bub}(t) + f_{sub}(t) + f_{sud}(t) \quad \text{(eq. S24)}$$

where *S(t)* is active site number related to time *t*, $f_{dis}(t)$, $f_{agg}(t)$, $f_{detach}(t)$, $f_{ad-dep}(t)$, $f_{bub}(t)$, $f_{sub}(t)$, and $f_{sud}(t)$ are the change rates of active site number caused by dissolution of catalyst, agglomeration, detachment of catalyst, adsorption/redeposition blocking, bubble blocking, substrate dissolution, and sudden failures by other effects.

As discussed above, $f_{dis}(t)$ could be expressed as

$$f_{dis}(t) = -k'S(t)^{x'} \quad \text{(eq. S25)}$$

Here we go further for the agglomeration effect. We used a sphere model to quantify the process:[15, 16]

$$\frac{dA}{dt} = -k_c(A - A_f) \quad \text{(eq. S26)}$$

$$A = k_{as}S(t) \quad \text{(eq. S27)}$$

$$f_{agg}(t) = \frac{dS_c}{dt} = -k_c(S(t) - S_f) \quad \text{(eq. S28)}$$

$$S_f = \frac{4\pi}{k_{as}}\left(\frac{S(t)\,M_{cat}}{\frac{4}{3}\pi\rho_{cat}}\right)^{\frac{2}{3}} \quad \text{(eq. S29)}$$

where *A* is surface area of the catalyst sphere, A_f is the final surface area after degradation, k_c is aggregation rate coefficient, k_{as} is the coefficient between surface area of single catalyst sphere and the overall active site number, S_c is the active site number influenced by aggregation, S_f is the final active site number after degradation, π is the ratio of the circumference of a circle to its diameter, M_{cat} is the molar mass of catalyst, ρ_{cat} is the density of catalyst. By combining the above equation, we have:

$$f_{agg}(t) = -k_c\left(S(t) - \frac{4\pi}{k_{as}}\left(\frac{S(t)\,M_{cat}}{\frac{4}{3}\pi\rho_{cat}}\right)^{\frac{2}{3}}\right) \quad \text{(eq. S30)}$$

Even though we may detail all other effects by establishing appreciate (differential) equations, it will lead to a too complicated description for active site number. Moreover, after introducing the full-microkinetic analysis under steady-state approximation for OER, it leads to a more

dazzling description, with the OER reaction rate *r* formulated as:

$$r = (k_{12}k_{23}k_{34}k_{41} - k_{14}k_{43}k_{32}k_{21}) / [(k_{23}k_{34}k_{41} + k_{21}k_{34}k_{41} + k_{21}k_{32}k_{41} + k_{21}k_{32}k_{43}) + (k_{14}k_{43}k_{32} + k_{34}k_{41}k_{12} + k_{32}k_{41}k_{12} + k_{12}k_{43}k_{32}) + (k_{23}k_{14}k_{43} + k_{21}k_{14}k_{43} + k_{41}k_{12}k_{23} + k_{43}k_{12}k_{23}) + (k_{14}k_{23}k_{34} + k_{34}k_{21}k_{14} + k_{32}k_{21}k_{14} + k_{12}k_{23}k_{34})] \quad \text{(eq. S31)}$$

in which k_{ij} is rate coefficient. For more details about the full OER kinetic analysis, please refer to discussion for OER microkinetics in the beginning of Part 1.

Therefore, to contribute to our proof-of-concept about OER performance degradation by data assimilation, it is necessary to simplify the model as possible and focus on one typical degradation mechanism.

To the end, in this work, apart from the dissolution of catalyst, we excluded other possible influences on the degradation process by elaborately designing our experiment (see more details in the above discussion for **Figure S1**). Therefore, we finally ascribed the degradation during OER mainly to the catalyst dissolution.

Part 2. Experimental and fitting results

We tested the influence of environmental temperature on the degradation experiment (**Figure S2** below). It is evident that the uncontrollable fluctuations of environmental temperature remarkably affected accurate collection of degradation data. This will hinder the effective forecasting by our DA-based method as proof-of-concept. Thus, we modified the experimental configuration to sustain the cell temperature with adding a temperature controller (*e.g.*, water bath), as a typical configuration shown in **Figure S3**. After excluding the obvious temperature fluctuations during OER degradation testing, the quality of experimental data was highly improved (*e.g.*, **Figure S6b**). Of course, we understand that even after the above improvement of our experimental configuration, there are still systemic errors such as the drift of reference electrode potential during the testing. For example, we found that the reference electrode potential was shifted by ~1 mV after degradation testing for the result in **Figure 2c** in main text. The 1 mV was small, but we still could not ensure the possible fluctuation of the reference electrode potential during the whole degradation testing. Nonetheless, the DA method enables to include those error effects in the algorithm to some extent, as the observation noises empirically defined in equation (8) and equation (9) in the Experimental Methods. Together with our rational design of degradation experiment to lower the environmental effects, the above advantage of DA contributes to reducing the systemic errors as possible and thus benefit the improvement of accuracy for lifetime forecasting.

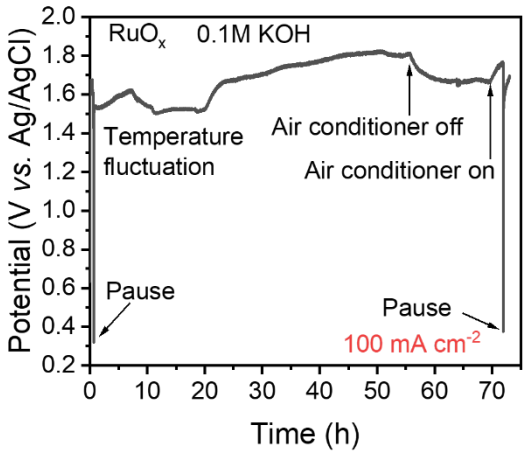

Figure S2. OER degradation testing under an atmosphere condition without controlling the reaction temperature. Current density was set at 100 mA cm^{-2} to monitor the applied potential during testing in 0.1 M KOH.

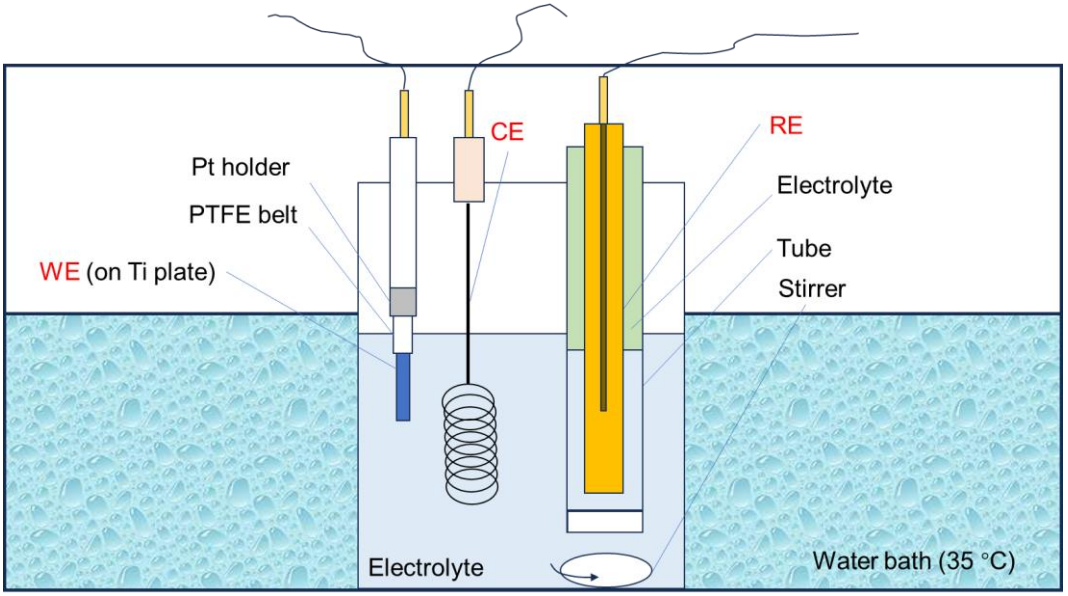

Figure S3. The three-electrode configuration in a water bath (35 °C). WE: Working electrode, CE: counter electrode, RE: reference electrode. PTFE: Polytetrafluoroethylene. The RE was positioned in a tube full of electrolyte, underneath which there was a magnetic stirrer at 600 rpm during the electrochemical measurement.

As we know, electrochemical processes typically include three main polarization mechanisms: activation, ohmic, and concentration effects. However, to make it more concise, we just used the Butler-Volmer equation according to the actual considerations: 1) we carried out iR compensation for the polarization curves. Thus, it is not necessary to consider the ohmic polarization in our analysis; 2) the reactant for OER is mainly water molecule for the condition in **Figure 2a** in the main text.[17] Due to the ultrahigh concentration of water molecules in an aqueous solution (typically > 50 M), the limiting current density for OER (> 5 A cm^{-2}, as estimated in a static condition with diffusion coefficient of H_2O: 2.57×10^{-9} m^2 s^{-1}, thickness of diffusion layer: 0.5 mm) is much higher than the current density range explored in our work (< 400 mA cm^{-2}).[17, 18] In addition, we carried out fierce stirring during the testing (**Figure S3**). Hence, the concentration-induced effect could be kindly ignored practically.

Furthermore, we empirically took the Butler-Volmer framework for the polarization curve in our study. According to our experimental result (**Figure 2a** in the main text), the experimentally-acquired polarization curves could be well quantified by the concise equation (3) in the main text. In addition, the double-layer charging current indicated the trend of active site number (**Figure 2b** in the main text): decreasing active site number during the degradation. Thus, by combing the above two results, we successfully achieved an initial verification of our proposed degradation model.

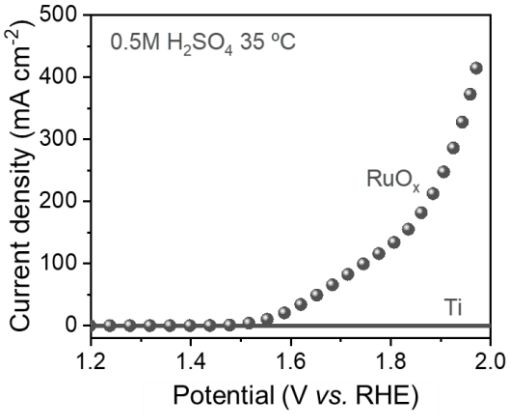

Figure S4. Polarization curves of Ti substrate (scan rate: 5 mV s^{-1}) and RuO_x (scan rate: 1 mV s^{-1}) in 0.5 M H_2SO_4 at 35 °C.

Table S1. Fitting parameters for the OER polarization curve with RuO_x as electrocatalyst in 0.5 M H_2SO_4 at 35 °C. F = 96485 C mol^{-1}, E_0 = 1.221 V (*vs.* RHE), R = 8.314 $J\cdot K^{-1}\cdot mol^{-1}$, T = 308 K.

I_0 / mA cm^{-2}	α_0	Adjusted R-square
2.358 ± 0.063	0.182 ± 0.001	0.99495

We carried out cyclic voltammetry (CV) measurements with various scan rates (**Figure S5**) to evaluate the double-layer capacitances (C_{dl}) of Ti substrate and RuO_x loaded on Ti substrate through:[19]

$$\frac{J_a - J_c}{2} = C_{dl}\upsilon \qquad \text{(eq. S32)}$$

where J_a is the current with an anodic scan, J_c is the current with a cathodic scan, υ is the scan rate. The half difference between J_a and J_c aimed to obtain the C_{dl} charging current with minimizing the background noise.

It showed that the C_{dl} of RuO_x on Ti substrate was much higher than that of Ti substrate (**Figure S5**c), indicating that the contribution of Ti substrate for the measured C_{dl} in RuO_x-loaded Ti substrate was ignorable. As reported previously, C_{dl} was associated with active site number,[20] thus change of C_{dl} charging current could be used to monitor the change of active site number through C_{dl} based on eq. S32. To simplify the measurement, we used C_{dl} charging current at a scan rate of 100 mV s^{-1} to track the active site number of RuO_x for OER during electrocatalyst degradation process.

A further explanation for using charging current to monitor the trend of active site number during the OER degradation is shown below.

Because of the difficulty in precisely determining the specific double-layer capacitance of the electrocatalyst in our work, we did not use electrochemically active surface area (ECSA), but instead using the charging current to track the trend of active site number change during degradation. This indirect method for monitoring active site number was based on the positive corelation among charging current, double-layer capacitance, actual reactive surface area, and active site number.[20, 21]

Note that the sites would be partially catalytically passivated during the reaction. To minimize this effect by OER, we carried out the testing for charging current during a non-Faradaic region (centred at 0.35 V (*vs.* Hg/Hg_2SO_4) with the potential window of 0.1 V) after pausing the degradation measurement. The same operations were conducted for all the charging currents in **Figure 2b** in the main text to get a reliable sketch for the trend of active site number.

In addition, the positive correlation between charging current and active site number could be further verified by the consistency among the decreased charging current after degradation (**Figure 2b** in the main text), the obvious disappearance of the catalyst layer after the degradation testing (**Figure S1**), and the decreased amount of Ru by ICP-OES (before testing: 0.135 mg cm^{-2}, after testing: 0.06 mg cm^{-2}).

Therefore, in our work we chose the charging current method to monitor the overall trend of active site number during OER degradation, for demonstrating an initial verification of our catalyst dissolution-dominated degradation model.

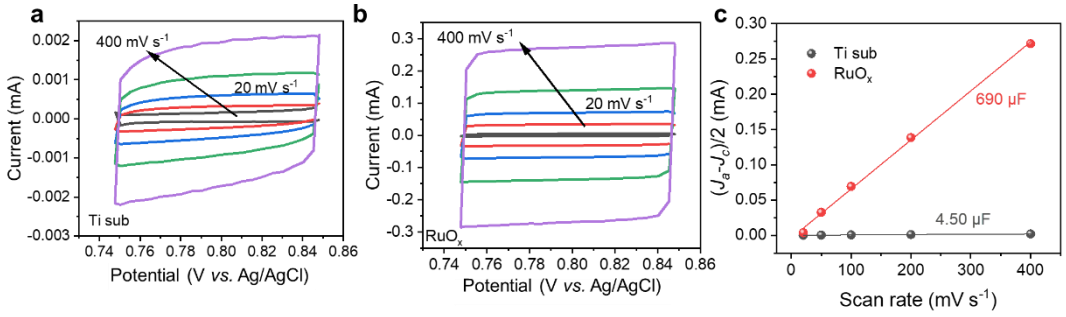

Figure S5. Non-Faradaic currents with CV in different scan rates (20, 50, 100, 200, 400 mV s^{-1}) between 0.75 V and 0.85 V (*vs.* AgCl) for (a) Ti substrate (Ti sub) and (b) RuO_x loaded on Ti substrate in 0.5 M H_2SO_4 at room temperature. (c) The half difference of CV currents at 0.80 V (*vs.* AgCl) between anodic (J_a) and cathodic (J_c) scans changing with various scan rates, through which double-layer capacitances (C_{dl}) were obtained: 4.50 μF for Ti substrate and 690 μF for RuO_x loaded on Ti substrate.

Table S2. Fitting parameters for the OER electrocatalyst degradation with RuO_x as electrocatalyst in 0.5 M H_2SO_4 at 35 °C (current density: 300 mA cm^{-2}) by our degradation model. I = 0.15 A, c = 1×10^{-6} A, S_{max} = 1.25×10^{-6} mol, R_0 = 0.9495 Ω, $r_{RWE,1}$ = 0 Ω h^{-1}.

α / V^{-1}	k_0 / A mol^{-1}	$k' \times 10^8$ / h^{-1}	x'	Adjusted R-square
5.907 ± 0.081	241.017 ± 22.346	3.5746 ± 0.0002	-0.1634 ± 0.0001	0.98977

[1]As for the parameter c (substrate current), given that the potential range was at ~1.3 V *vs.* Hg/Hg_2SO_4 (*i.e.*, ~2.0 V *vs.* RHE) in the majority of the degradation process (**Figure 2**c) and the Ti substrate showed a current at a magnitude of 1×10^{-6} A at this potential range (calculated from the current density in **Figure S4**), herein we set c as a constant of 1×10^{-6} A during the whole degradation period.

[2] The change of resistance was ignorable (before and after degradation: R_u was 0.947 Ω and 0.952 Ω, respectively), thus we set the rate of resistance change $r_{RWE,1}$ as 0 Ω h^{-1} and took R_0 as the average of R_u before and after durability testing (*i.e.*, R_0 = 0.9495 Ω). Similar treatments were conducted for fitting other degradation curves in this work.

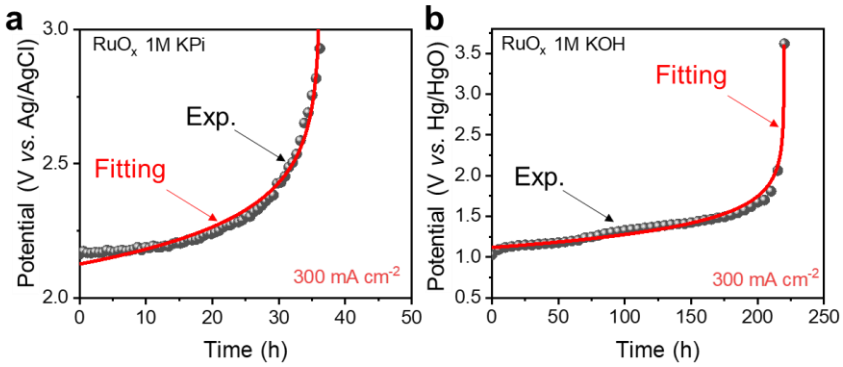

Figure S6. (a) OER electrocatalyst degradation and the corresponding fitting by our degradation model (**Table S3**); electrolyte: potassium phosphate buffer (1 M KPi, pH 7) at 35 °C. (b) OER electrocatalyst degradation and the fitting in an alkaline condition (1 M KOH, pH 14) at 35 °C (**Table S4**).

Table S3. Fitting parameters for the OER electrocatalyst degradation with RuO_x as electrocatalyst in 1 M KPi at 35 °C (current density: 300 mA cm^{-2}) by our degradation model. $I = 0.15$ A, $c = 1\times10^{-6}$ A, $S_{max} = 1.25\times10^{-6}$ mol, $R_0 = 1.915$ Ω, $r_{RWE,1} = 0$ Ω h^{-1}.

α / V^{-1}	k_0 / A mol^{-1}	$k' \times 10^8$ / h^{-1}	x'	Adjusted R-square
5.553 ± 0.037	4.414 ± 0.313	1.7588± 0.0015	-0.0463 ± 0.0001	0.97684

Table S4. Fitting parameters for the OER electrocatalyst degradation with RuO_x as electrocatalyst in 1 M KOH at 35 °C (current density: 300 mA cm^{-2}) by our degradation model. $I = 0.033$ A, $c = 1\times10^{-6}$ A, $S_{max} = 2.75\times10^{-7}$ mol, $R_0 = 2.393$ Ω, $r_{RWE,1} = 0$ Ω h^{-1}.

α / V^{-1}	k_0 / A mol^{-1}	$k' \times 10^6$ / h^{-1}	x'	Adjusted R-square
6.452 ± 0.094	148.765 ± 16.898	1.0149 ± 0.0001	0.4087 ± 0.0001	0.93754

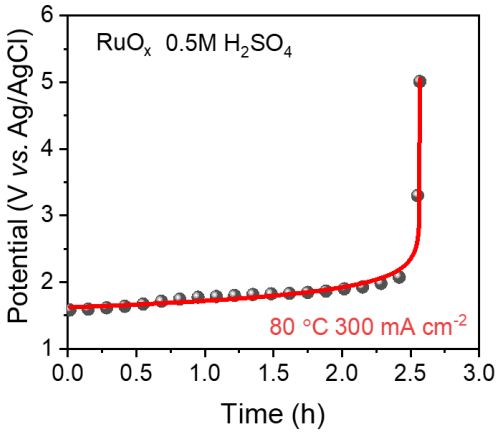

Figure S7. OER electrocatalyst degradation and the fitted plot by our degradation model in 0.5 M H_2SO_4 at 80 °C (**Table S5**). The testing was implemented in a heating mantle.

Table S5. Fitting parameters for the OER electrocatalyst degradation with RuO_x as electrocatalyst in 0.5 M H_2SO_4 at 80 °C (current density: 300 mA cm^{-2}) by our degradation model. I = 0.15 A, c = 1×10^{-6} A, S_{max} = 1.25×10^{-6} mol, R_0 = 0.971 Ω, $r_{RWE,1}$ = 0 Ω h^{-1}.

α / V^{-1}	k_0 / A mol^{-1}	$k' \times 10^8$ / h^{-1}	x'	Adjusted R-square
4.298 ± 0.211	211.447 ± 72.371	4.5582 ± 0.0026	-0.1632 ± 0.0001	0.96816

Table S6. Fitting parameters for the OER electrocatalyst degradation with MnO_x as electrocatalyst in 1 M KPi at 35 °C (current density: 50 mA cm^{-2}) by our degradation model. I = 0.025 A, c = 1×10^{-6} A, S_{max} = 1.25×10^{-6} mol, R_0 = 2.67 Ω, $r_{RWE,1}$ = 0 Ω h^{-1}.

α / V^{-1}	k_0 / A mol^{-1}	$k' \times 10^8$ / h^{-1}	x'	Adjusted R-square
0.264 ± 0.002	6502.405 ± 58.588	2.9402 ± 0.1449	-0.2765 ± 0.0039	0.99984

Table S7. Fitting parameters for the OER electrocatalyst degradation with NiO_x as electrocatalyst in 1 M KPi at 35 °C (current density: 50 mA cm^{-2}) by our degradation model. I = 0.025 A, c = 1×10^{-6} A, S_{max} = 1.25×10^{-6} mol, R_0 = 2.28 Ω, $r_{RWE,1}$ = 0 Ω h^{-1}.

α / V^{-1}	k_0 / A mol^{-1}	$k' \times 10^9$ / h^{-1}	x'	Adjusted R-square
0.158 ± 0.004	11169.690 ± 188.909	5.9800 ± 2.1558	-0.3531 ± 0.0280	0.99889

Table S8. Fitting parameters for the OER electrocatalyst degradation with FeO_x as electrocatalyst in 1 M KPi at 35 °C (current density: 50 mA cm^{-2}) by our degradation model. I = 0.025 A, $c = 1\times10^{-6}$ A, $S_{max} = 1.25\times10^{-6}$ mol, R_0 = 3.08 Ω, $r_{RWE,1}$ = 0 Ω h^{-1}.

α / V^{-1}	k_0 / A mol^{-1}	$k' \times 10^8$ / h^{-1}	x'	Adjusted R-square
0.560 ± 0.010	4875.934 ± 165.792	2.6251 ± 0.0016	-0.1806 ± 0.0002	0.98735

Table S9. Fitting parameters for the OER electrocatalyst degradation with CoO_x as electrocatalyst in 1 M KPi at 35 °C (current density: 50 mA cm^{-2}) by our degradation model. I = 0.025 A, $c = 1\times10^{-6}$ A, $S_{max} = 1.25\times10^{-6}$ mol, R_0 = 2.19 Ω, $r_{RWE,1}$ = 0 Ω h^{-1}.

α / V^{-1}	k_0 / A mol^{-1}	$k' \times 10^{10}$ / h^{-1}	x'	Adjusted R-square
0.459 ± 0.007	3682.010 ± 103.252	7.7856 ± 0.0184	-0.4291 ± 0.0004	0.99597

Table S10. Fitting parameters for the OER electrocatalyst degradation with M as electrocatalyst in 1 M KPi at 35 °C (current density: 300 mA cm^{-2}) by our degradation model. I = 0.15 A, $c = 1\times10^{-6}$ A, $S_{max} = 1.25\times10^{-6}$ mol, R_0 = 2.63 Ω, $r_{RWE,1}$ = 0 Ω h^{-1}.

α / V^{-1}	k_0 / A mol^{-1}	$k' \times 10^9$ / h^{-1}	x'	Adjusted R-square
0.277 ± 0.016	71138.509 ± 2926.961	4.7704 ± 0.2010	-0.5039 ± 0.0048	0.99355

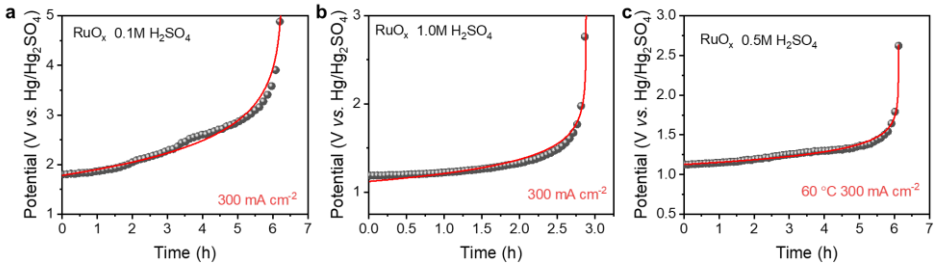

Figure S8. OER electrocatalyst degradation in (a) 0.1 M H_2SO_4 at 35 °C, (b) 1.0 M H_2SO_4 at 35 °C, and (c) 0.5 M H_2SO_4 at 60 °C. Spheres: experimental data, lines: fitting results.

Table S11. Fitting parameters for the OER electrocatalyst degradation with RuO_x as electrocatalyst in 0.1 M H_2SO_4 at 35 °C (current density: 300 mA cm^{-2}) by our degradation model. I = 0.15 A, c = 1×10^{-6} A, S_{max} = 1.25×10^{-6} mol, R_0 = 4.67 Ω, $r_{RWE,1}$ = 0 Ω h^{-1}.

α / V^{-1}	k_0 / A mol^{-1}	$k' \times 10^8$ / h^{-1}	x'	Adjusted R-square
1.232 ± 0.019	31605.160 ± 1016.310	1.6434 ± 0.0002	-0.1718 ± 0.0001	0.96381

Table S12. Fitting parameters for the OER electrocatalyst degradation with RuO_x as electrocatalyst in 1.0 M H_2SO_4 at 35 °C (current density: 300 mA cm^{-2}) by our degradation model. I = 0.15 A, c = 1×10^{-6} A, S_{max} = 1.25×10^{-6} mol, R_0 = 0.545 Ω, $r_{RWE,1}$ = 0 Ω h^{-1}.

α / V^{-1}	k_0 / A mol^{-1}	$k' \times 10^8$ / h^{-1}	x'	Adjusted R-square
3.755 ± 0.161	2420.052 ± 465.169	1.0106 ± 0.0003	-0.2596 ± 0.0002	0.92865

Table S13. Fitting parameters for the OER electrocatalyst degradation with RuO_x as electrocatalyst in 0.5 M H_2SO_4 at 60 °C (current density: 300 mA cm^{-2}) by our degradation model. I = 0.15 A, c = 1×10^{-6} A, S_{max} = 1.25×10^{-6} mol, R_0 = 1.025 Ω, $r_{RWE,1}$ = 0 Ω h^{-1}.

α / V^{-1}	k_0 / A mol^{-1}	$k' \times 10^8$ / h^{-1}	x'	Adjusted R-square
5.617 ± 0.077	505.459 ± 42.490	1.3597 ± 0.0001	-0.1868 ± 0.0001	0.97284

Of course, we could not completely exclude other degradation mechanism except catalyst dissolution. As the discussion for **Figure S1**, we mainly ascribed the degradation during OER to the catalyst dissolution in this work after kindly designing the experimental configuration to demonstrate our proof-of-concept toward quantifying OER performance degradation. Nonetheless, in principle using particular parameter in our model is hard to cover the real underlying cause for the overall degradation process under various conditions. However, from the practical degradation results under various current densities (25, 50, 100 mA cm^{-2} in **Figure S9** below; 300 mA cm^{-2} in **Figure 2c** in the main text), our present degradation model enabled to describe the OER degradation with a wide-range current density to some extent. In addition, according to the model diagnosis (**Figure S11**), the parameters related to OER mechanism (*i.e.*, α and k_0) showed no significant change during the whole degradation process; in contrast, the dissolution factor k' changed a lot, indicating that the dissolution factor was an important parameter during the degradation and a more comprehensive consideration for the dissolution kinetics is expected in future. To avoid misunderstanding, we underline that the dissolution factor should be treated as "apparent" parameter.

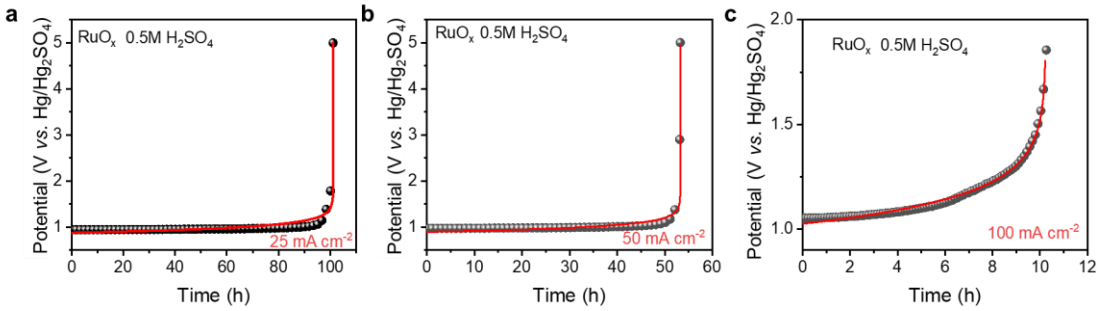

Figure S9. OER electrocatalyst degradation in 0.5 M H_2SO_4 under 35 °C and the corresponding fitting by our degradation model at (a) 25 mA cm^{-2}, (b) 50 mA cm^{-2}, and (c) 100 mA cm^{-2}, respectively.

Table S14. Fitting parameters for OER electrocatalyst degradation with RuO_x as electrocatalyst in 0.5 M H_2SO_4 at 35 °C (current density: 25 mA cm^{-2}) by our degradation model. I = 0.0125 A, $c = 1\times10^{-6}$ A, $S_{max} = 1.25\times10^{-6}$ mol, R_0 = 1.105 Ω, $r_{RWE,1}$ = 0 Ω h^{-1}.

α / V^{-1}	k_0 / A mol^{-1}	$k' \times 10^8$ / h^{-1}	x'	Adjusted R-square
8.641 ± 0.506	5.735 ± 2.856	1.9723 ± 0.0006	0.03199 ± 0.00002	0.6456

Table S15. Fitting parameters for OER electrocatalyst degradation with RuO_x as electrocatalyst in 0.5 M H_2SO_4 at 35 °C (current density: 50 mA cm^{-2}) by our degradation model. I = 0.025 A, $c = 1\times10^{-6}$ A, $S_{max} = 1.25\times10^{-6}$ mol, R_0 = 1.095 Ω, $r_{RWE,1}$ = 0 Ω h^{-1}.

α / V^{-1}	k_0 / A mol^{-1}	$k' \times 10^8$ / h^{-1}	x'	Adjusted R-square
8.707 ± 0.467	10.627 ± 4.852	1.4069 ± 0.0005	-0.03509 ± 0.00002	0.8608

Table S16. Fitting parameters for OER electrocatalyst degradation with RuO_x as electrocatalyst in 0.5 M H_2SO_4 at 35 °C (current density: 100 mA cm^{-2}) by our degradation model. I = 0.023 A, $c = 1\times10^{-6}$ A, $S_{max} = 5.75\times10^{-7}$ mol, R_0 = 1.399 Ω, $r_{RWE,1}$ = 0 Ω h^{-1}.

α / V^{-1}	k_0 / A mol^{-1}	$k' \times 10^8$ / h^{-1}	x'	Adjusted R-square
6.950 ± 0.043	39.957 ± 1.871	1.5911 ± 0.0050	-0.08222 ± 0.00003	0.9917

To further demonstrate the capability of our DA-based method for lifetime forecasting, we carried out DA for ~40-h and ~200-h testing, as the results shown in **Figure S10**. It is evident that with increasing the assimilation window, the forecasted degradations approached to the experimental results with forecast errors reduced, indicating continuously improved forecast accuracies. Through the above results for various lifetimes, we solidified a good capability of our DA-based method to forecast OER degradation.

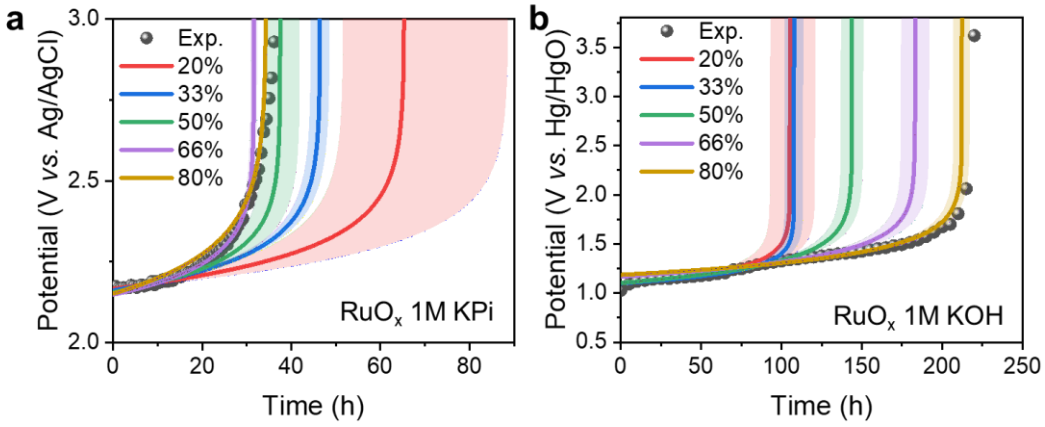

Figure S10. DAs for OER electrocatalyst degradation testing in (a) 1 M KPi and (b) 1 M KOH at 35 °C, respectively. The assimilation window varied from 20% to 80% of the whole experimental period.

Given the large error of lifetime forecasted by DA in the early degradation stage (**Figure 3**b in the main text), it is necessary to pinpoint the issues of the present degradation model for guiding future modification. To this end, exemplifying the DA results in **Figure 3**a in the main text, we demonstrated a model diagnosis by tracking key parameters with updating degradation data. Both parameters α and k_0 for the intrinsic OER activity remained almost unchanged, indicating that the considerations for these two parameters in our model were reliable (**Figure S11**). As discussed, k_0 was related to the energetic span δG (eq. (S11-2) and eq. (S13-2) in the SI). However, the implementation of δG was based on a simplification by using the maximum term in a reaction rate.[4, 5] Another simplification for δG in this work originated from its first-order approximation of the Taylor polynomial, leading to a linear approximation of the relationship between δG and the potential E. These two main simplifications could lead to an unavoidable model error for OER electrocatalyst degradation, resulting in obvious errors of k_0 in the dynamic DA (**Figure S11**b). Fortunately, the steady trend of k_0 illustrated that the energetic span-based kinetic model was still applicable even under strong approximations.

In contrast to the stable trends of both α and k_0, the dissolution factor k' for active site dissolution increased with the growing assimilation window (**Figure S11**c), indicating that k' was a particularly important parameter for accurate forecasting. The increase of k' with the expanded assimilation window implied promoted dissolution of the electrocatalyst during degradation. This was consistent with the exponentially declining double-layer charge current (*i.e.*, the active site number) during degradation (**Figure 2**b in the main text). However, as suggested by the obvious change of k', the excessed simplification in electrocatalyst dissolution picture based on the semi-empirical rate law contains issues to comply with the actual process.

A more detailed consideration for active site dissolution could be needed, shown by regarded electrocatalyst dissolution as a side reaction via a common intermediate in the microkinetic network.[22] Besides, possible chemical dissolution of electrocatalytic species may also be included.[23] Apart from the above dissolution effects, some other factors to reduce active site number, as discussed in Part 1 in the SI, may be contained. For example, agglomeration of surface-active species during long-term testing would diminish the electrochemically active surface area, which in turn reduced active site number for OER.[24]

Although several microscopic effects need to be included in the kinetic model to further improve the forecasting accuracy, by using DA with the degradation model in this work, reliable forecast of anode lifetime towards OER was successfully demonstrated. Our method thus demonstrated improved forecast ability with the degradation phenomena proceeding, with an additional discovery of the dominating factor in our present degradation model. We believe that this DA-based framework for lifetime forecasting will be inspiring to accelerate the assessment of long-term performance for oxygen electrocatalysis-based energy conversion systems.

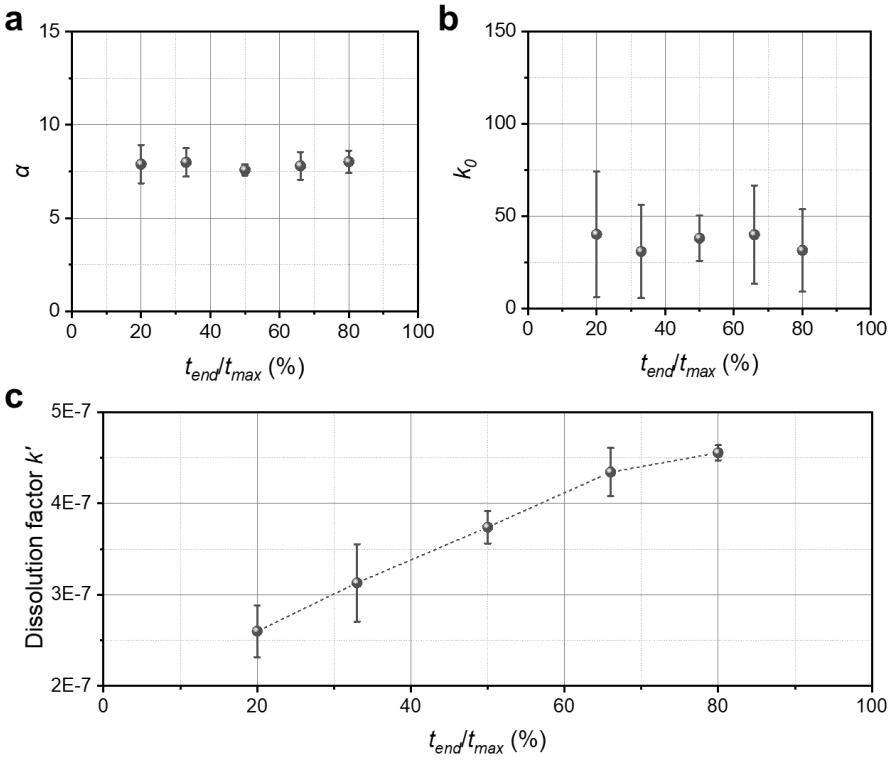

Figure S11. Diagnosis of the degradation model by monitoring the parameters for (a) α, (b) k_0, and (c) dissolution factor k' in our degradation model by dynamic DAs with various assimilation windows (from 20% to 80% of the whole experimental period). The error bars were obtained by conducting DA for five times.

As for the assimilation window size, we compared various sizes from 300 h to 600 h and found that the 600-h forecast achieved a negligible discrepancy (**Figure S12**a). It is evident that the overall trend showed an improvement of the forecast ability with increasing the assimilation size (**Figure S12**b). A little larger forecast errors for 400-h and 500-h DA than the 300-h DA should be caused by the "abrupt change" of the collected data between 320 h and 370 h. This abrupt change might result from unpredictable external disturbance from the environment during the long-term testing under 80 °C. However, the satisfying forecasting by the 600-h assimilation window took around two thirds of the whole testing period, while the shorter 300-h window showed a relatively large forecast error. Thus, we picked up the short 300-h assimilation window and carried out smoothing until 400 h for data pretreatment to minimize the influence by the abrupt change as mentioned above. This benefited the forecasting with an acceptable forecast error within 10% (**Figure S15**). Therefore, in this work we focused on the 300-h assimilation window for demonstrating the practical applicability of our DA-based method.

The discrepancy for the 300-h assimilation window-based forecasting is below 10% of the forecast error (**Figure S15**). This present result within 10%-forecast error is sufficiently acceptable as our method inspired by weather forecasting which generally has accuracy of around 90% in a short-term (five-day) forecast and lower in longer forecasts.[25, 26]

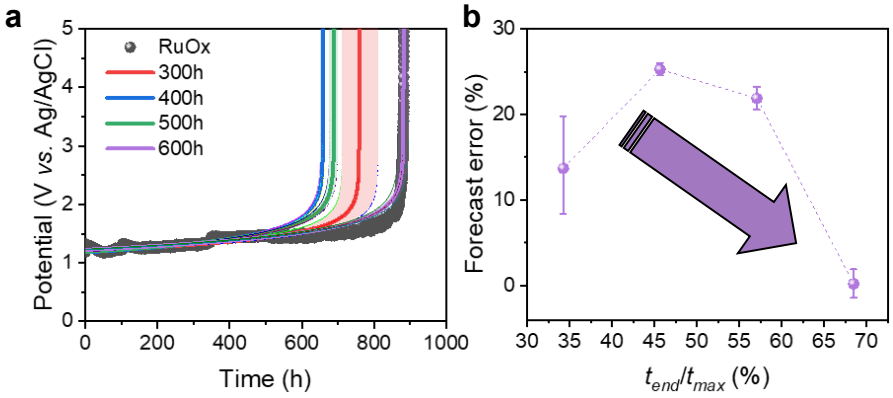

Figure S12. (a) Lifetime forecasting for long-term durability by DA with 300~600 h as the assimilation window, respectively, and (b) the trend of forecast error with increasing the assimilation window. No smooth pretreatment.

About the degradation process of OER, although in this work we did not get into atomic/electronic scale for a deeper understanding, we carried out the quantification of OER degradation process with a simple and practicable model (as detailed in Part 1 in the SI), combined with a rational design of the experiment. As a result, we could grasp the overall framework of OER degradation. We agree that this DA-based method still has some limitations, like the simplified degradation model that hindered a thorough understanding of the underlying processes. Another shortcoming by this simplified model is that it restricts our method for quantifying situations with the degradation process dominated by other factors, such as bubble blocking, substrate dissolution, and significant sudden failures. In addition, a full description of the OER microkinetics is expected to be involved for further improving our present model. Thus, specifically speaking, apart from the demanding for a more comprehensive dissolution model after the model diagnosis (**Figure S11**) and consideration of other degradation mechanisms, a higher-level-ladder description of the OER process is expected to understand the structure evolution of electrode-electrolyte interface during degradation as well as the resultant effects. This level-up OER degradation model may include reaction thermodynamics, microkinetics, mass transport effect, electric double layer effect, and even the reconstruction of catalyst during the reaction.[7, 8] However, the above points are still challenging at present and more endeavours will be conducted in our future work.

As for reinforcement learning (RL), it is a concept rather similar to Bayesian optimization or genetic algorithms, and can be considered a type of optimization technique. RL aims to obtain the optimal policy with the largest cumulative rewards, *i.e.*, the optimization of "process". On the other hand, DA is a technique to integrate experimental data and numerical calculation/simulation results. In particular, the non-sequential DA method integrates them through optimization of the model parameters, which allows extrapolation of the model (*i.e.*, the forecasting). Therefore, it is difficult to compare DA and RL because their intended uses are different. In addition, the DA method used in this study only needs to minimize the data misfit between model-generated and experimental data, and does not need optimization of the "process" itself (*i.e.*, the degradation process). Hence, the advantage of RL would not lead to improve the accuracy of the forecasting provided in this study.

All in all, the extrapolation capability of our model showed an overall rising general tendency with increasing the assimilation window. Benefited by the effective description on the OER degradation with our proposed model and the consideration of the non-uniform experimental uncertainties in DA, as a result, even a small part of data enables to obtain satisfying forecasting for anode lifetime. For example, we achieved a good lifetime forecast with error below 10% just by 34% of the assimilation window (*i.e.*, 34% of the whole data), as shown in **Figure S14**.

This is exactly one of the advantages of our method as compared to other methods like machine learning that usually requires massive datasets for training.

For a comprehensive comparison of our method with other typical methods:

To obtain a good forecast of the electrocatalyst lifetime, the parameters in the OER model should be identified with minimal experiments. Several approaches exist for identifying the parameters in a numerical model. The most reasonable approach is identification based on the physically well-established theory. However, it is still challenging to derive an omniscient theory to fully describe the OER degradation. Theoretical calculations and/or numerical simulations (*e.g.*, *ab initio* calculations and molecular dynamics simulation) are also effective for the determination of parameters in chemical reactions, but these approaches can be highly time-consuming works. Moreover, they have limitations such as available temperature and timescale, or computational cost.

Another promising approach is to identify the parameters based on experimental results. One of the simplest ways of this approach is to fit the model to the experimental result by optimizing the parameters. Mathematically, the non-sequential DA methods can be regarded as extended fitting methods based on the Bayesian inference. Therefore, the DA provides better parameter optimization than the simple fitting, especially when the experimental results and numerical models have non-uniform uncertainties. For a detail discussion between the DA and fitting results please refer to the part for **Figure 3c** in the main text.

Machine learning is also a candidate for a parameter identification method. Although machine learning can predict the learned phenomena in a short time, it requires huge amounts of data (typically thousands or more) for training. Given the anode lifetime in the OER testing, the machine learning approach cannot be employed because of the difficulty in preparing sufficient training data.

As aforementioned, the DA is expected to provide better identifications than the simple fitting. Therefore, we compared the lifetime forecasting by the DA and fitting (**Figure S14,S15**). Comparing the case using the experimental data up to 300 h, the forecast error for the DA is 4%, while that for the fitting is ~60%. Moreover, the fitting approach requires experimental data up to approximately the same time as the lifetime to forecast as accurately as the DA. These results clearly demonstrates that our approach employing DA is more promising and practical usefulness than the existing approach in forecasting the anode lifetime using the OER degradation model.

Furthermore, we demonstrated machine learning (ML)-based methods to forecast the lifetime. We used the data in **Table S17** for training ML models by three typical algorithms: linear regression, gradient boosting, and random forest (**Figure S13**a). The trained ML models were then used to forecast the lifetime of the long-term testing in **Figure S14**). As shown in **Figure S13**b, all the ML-based methods used here showed poor forecast accuracies with significantly large forecast errors (almost 80%). This should result from the too-small size of the dataset to carry out sufficient trainings of the ML models for minimizing underfitting or overfitting. In contrast, our DA method performed well for lifetime forecasting (forecast error < 10%) under the same size of dataset. This is exactly the attractive merit of the DA-based method: not too much data to obtain reliable forecasting by integrating the knowledge-embedded model (*i.e.*, the degradation model).

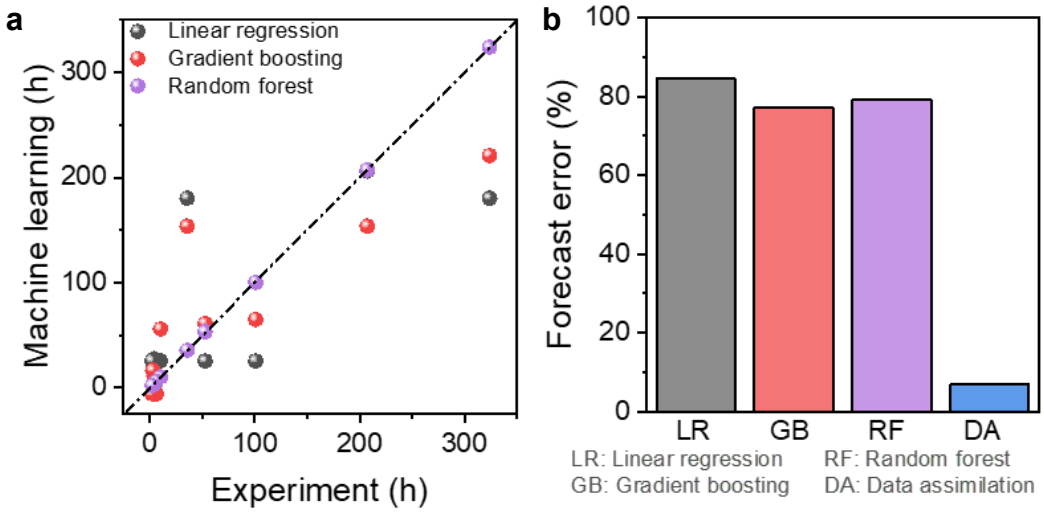

Figure S13. Comparison between ML and DA methods for lifetime forecasting. (a) Training the ML models by using the dataset in **Table S17** and the comparison between the modelled and the experimental lifetimes. Three typical algorithms for ML were used: linear regression, gradient boosting, and random forest. (b) Forecast errors of the trained ML models and our DA method for the long-term testing in **Figure S14**. For convenience, here the time at the potential increased by 0.7 V from the beginning was set as the "lifetime".

Table S17. Experimental conditions as descriptors for lifetime forecasting in the ML algorithms. The lifetime here was set as the time at the potential increased by 0.7 V from the beginning. Electrocatalyst: RuO_x.

Current density / mA cm^{-2}	**Cation atomic mass** (electrolyte)[1]	**Anion mass 1** (electrolyte)[2]	**Anion mass 2** (electrolyte)[3]	**Electrolyte Concentration /** mol L^{-1}	**pH**	**Temperature** / °C	**Lifetime** / h
100	39	31	95	1	7.076	35	323.9
25	1	32	96	0.5	0.346	35	101
50	1	32	96	0.5	0.343	35	52.7
100	1	32	96	0.5	0.374	35	10.2
300	39	31	95	1	7.094	35	35.6
300	1	32	96	0.1	0.868	35	4
300	1	32	96	1	-0.003	35	2.8
300	1	32	96	0.5	0.274	60	6.1
300	1	32	96	0.5	0.4	80	2.1
300	39	17	17	1	14	35	207.3

[1]For KPi (potassium phosphate) and KOH it is the atomic mass of K, for H_2SO_4 it is the atomic mass of H.

[2]For KPi it is P, for H_2SO_4 it is S, for KOH it is OH.

[3]For KPi it is PO_4, for H_2SO_4 it is SO_4, for KOH it is OH.

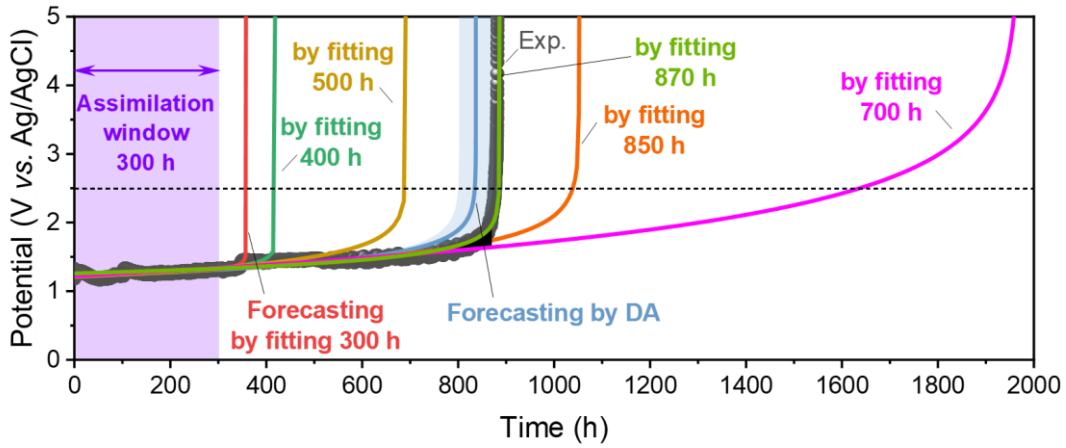

Figure S14. Lifetime forecasting for long-term durability by DA with 34% (*i.e.*, 300 h) of the whole data, as well as the forecasting based on simple fittings by using various data lengths including 34% (300 h), 46% (400 h), 57 % (500 h), 80% (700 h), 97 % (850 h), and 99% (870 h). Experimental condition: 0.1 M sodium carbonate (pH 9.2) at 80 °C under 100 mA cm^{-2}, with RuO_x as the electrocatalyst for OER.

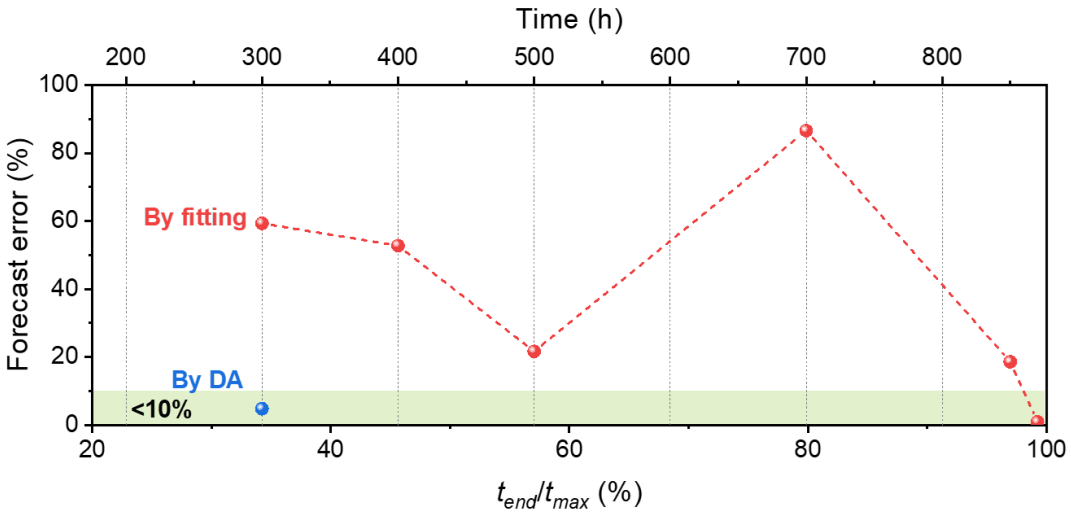

Figure S15. Trend of the forecast errors with various data lengths by simple fittings from 34% to 99 % of the whole measurement period (noted as t_{end}/t_{max}). The forecast error by DA was also shown for comparison.

Table S18. Fitting parameters for the OER electrocatalyst degradation with RuO_x as electrocatalyst in 0.1 M sodium carbonate (pH 9.2) at 80 °C (current density: 100 mA cm^{-2}) by our degradation model. I = 0.02 A, c = 1×10^{-6} A, S_{max} = 6.25×10^{-7} mol, R_0 = 8.6 Ω, $r_{RWE,1}$ = 0 Ω h^{-1}. Experimental data used for fitting: 300 h.

α / V^{-1}	k_0 / A mol^{-1}	$k' \times 10^{11}$ / h^{-1}	x'	Adjusted R-square
16.289 ± 2.388	0.001 ± 0.003	5.688 ± 8.025	-0.2255 ± 0.1041	0.41168

Table S19. Fitting parameters for the OER electrocatalyst degradation with RuO_x as electrocatalyst in 0.1 M sodium carbonate (pH 9.2) at 80 °C (current density: 100 mA cm^{-2}) by our degradation model. I = 0.02 A, c = 1×10^{-6} A, S_{max} = 6.25×10^{-7} mol, R_0 = 8.6 Ω, $r_{RWE,1}$ = 0 Ω h^{-1}. Experimental data used for fitting: 400 h.

α / V^{-1}	k_0 / A mol^{-1}	$k' \times 10^{10}$ / h^{-1}	x'	Adjusted R-square
12.4307 ± 0.300	0.069 ± 0.022	39.398 ± 3.971	0.0637 ± 0.0073	0.79713

Table S20. Fitting parameters for the OER electrocatalyst degradation with RuO_x as electrocatalyst in 0.1 M sodium carbonate (pH 9.2) at 80 °C (current density: 100 mA cm^{-2}) by our degradation model. I = 0.02 A, c = 1×10^{-6} A, S_{max} = 6.25×10^{-7} mol, R_0 = 8.6 Ω, $r_{RWE,1}$ = 0 Ω h^{-1}. Experimental data used for fitting: 500 h.

α / V^{-1}	k_0 / A mol^{-1}	$k' \times 10^{9}$ / h^{-1}	x'	Adjusted R-square
5.892 ± 0.144	70.982 ± 10.887	5.191± 6.080	0.2624 ± 0.0815	0.86046

Table S21. Fitting parameters for the OER electrocatalyst degradation with RuO_x as electrocatalyst in 0.1 M sodium carbonate (pH 9.2) at 80 °C (current density: 100 mA cm^{-2}) by our degradation model. I = 0.02 A, c = 1×10^{-6} A, S_{max} = 6.25×10^{-7} mol, R_0 = 8.6 Ω, $r_{RWE,1}$ = 0 Ω h^{-1}. Experimental data used for fitting: 700 h.

α / V^{-1}	k_0 / A mol^{-1}	$k' \times 10^{7}$ / h^{-1}	x'	Adjusted R-square
2.472 ± 1.872	2390.066 ± 4678.145	2.904 ± 39.260	0.4371 ± 0.9060	0.85557

Table S22. Fitting parameters for the OER electrocatalyst degradation with RuO_x as electrocatalyst in 0.1 M sodium carbonate (pH 9.2) at 80 °C (current density: 100 mA cm^{-2}) by our degradation model. I = 0.02 A, c = 1×10^{-6} A, S_{max} = 6.25×10^{-7} mol, R_0 = 8.6 Ω, $r_{RWE,1}$ = 0 Ω h^{-1}. Experimental data used for fitting: 850 h.

α / V^{-1}	k_0 / A mol^{-1}	$k' \times 10^9$ / h^{-1}	x'	Adjusted R-square
4.665 ± 0.089	224.839 ± 22.026	30.972 ± 9.540	0.2561 ± 0.0220	0.89794

Table S23. Fitting parameters for the OER electrocatalyst degradation with RuO_x as electrocatalyst in 0.1 M sodium carbonate (pH 9.2) at 80 °C (current density: 100 mA cm^{-2}) by our degradation model. I = 0.02 A, c = 1×10^{-6} A, S_{max} = 6.25×10^{-7} mol, R_0 = 8.6 Ω, $r_{RWE,1}$ = 0 Ω h^{-1}. Experimental data used for fitting: 870 h.

α / V^{-1}	k_0 / A mol^{-1}	$k' \times 10^{11}$ / h^{-1}	x'	Adjusted R-square
7.047 ± 0.054	15.056 ± 0.944	1249.26 ± 4.55	0.1867 ± 0.0004	0.91168

Even though the satisfactory application of our method in OER, one key limitation of the applicability to other electrochemical systems is our relatively simplified model. Our present model just focused on dissolution of catalyst for dominating the overall degradation. Other degradation mechanisms may influence or even dominate the overall degradation process. To demonstrate this consideration, we inspected the degradation for hydrogen evolution reaction (HER). As a result, the dissolution of the substrate, rather than the electrocatalyst, might dominate the overall degradation process (**Figure S16**) and this is beyond our present model. Therefore, for a wider application of our degradation model in the future, it is essential to build up a comprehensive model with various degradation factors.

Another limitation is that more factors should be considered from the present three-electrode system to practical electrolyzer with whole reaction (not just the half-reaction like OER or HER). Apart from the coupling of the different degradation processes between the half-reactions, the complicated configuration in electrolyzer will pose new challenges. For example, the influences of the configuration in ion-exchange membrane water electrolyzer, such as the structure of membrane electrode, pressure, and mass transport through the porous layer, will be more challenging to make a comprehensive and practically available degradation model.

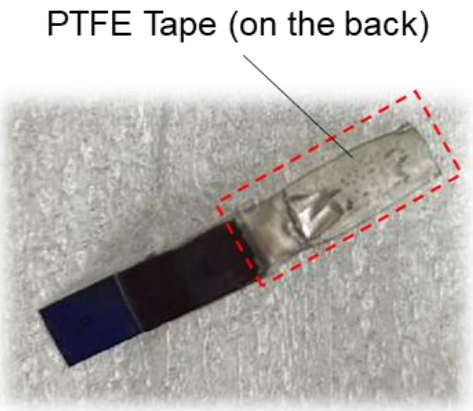

Figure S16. The Ti-based substrate after long-term degradation testing (chronopotentiometry) for HER. Working electrode: RuO_x loaded on Ti substrate, counter electrode: IrO_x-loaded Ti mesh, reference electrode: Hg/Hg_2SO_4 (saturated K_2SO_4), electrolyte: 0.5 M H_2SO_4, temperature: 35 °C, current density: 100 mA cm^{-2}. The polytetrafluoroethylene (PTFE) tape on the back was used to eliminate the current from the substrate for HER.

Part 3. Model interpretability and *degree of degradation control*

We tracked the dissolution factor (*k'*), as defined in our knowledge-contained degradation model, under various materials and conditions during the DA processes. A larger *k'* suggests a faster dissolution process. It showed that *k'* increased in order of materials FeO_x < CoO_x < NiO_x (**Figure S17**a), suggesting an ascending order of dissolution rate of FeO_x < CoO_x < NiO_x. This is consistent with the descending lifetime order of FeO_x > CoO_x > NiO_x (**Figure 2**d in the main text). The above relationship might be understood by the largest metal-oxygen bond dissociation energy of Fe, followed by Co then Ni,[27] *i.e.*, a stronger metal-oxygen bonding benefits a slower dissolution process for a longer anode lifetime. As for the degradations in different conditions (various pHs from acid to alkali), the dissolution factor *k'* increased in order of alkaline < neutral < acidic conditions (**Figure S17**b), implying promoted dissolution of electrocatalyst from alkali to acid. This result matched the lifetime trend of the electrocatalyst in different pH conditions: alkaline > neutral solution > acid (**Figure S6** and **Figure 2c**). All the above results further verified our dissolution-based degradation model and demonstrated its satisfying interpretability.

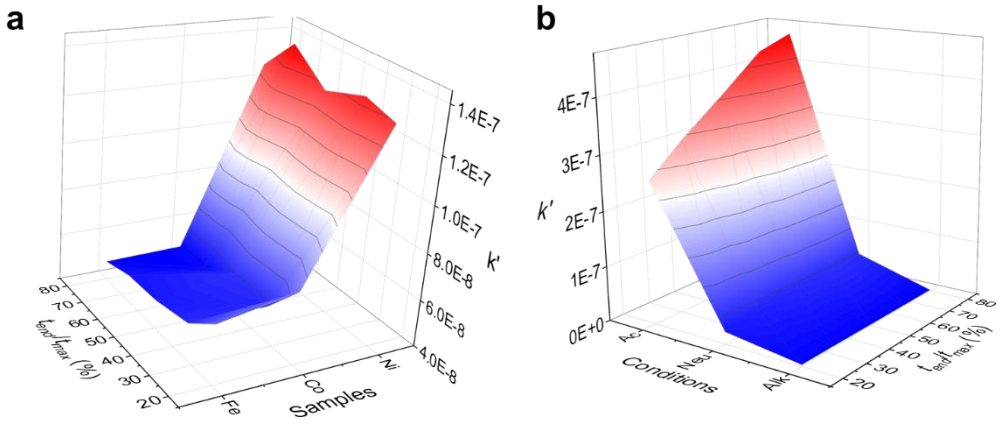

Figure S17. The dissolution factor *k'* derived from the DA method *via* different (a) materials (Fe: FeO_x, Co: CoO_x, Ni: NiO_x; 1 M KPi at 35 °C, current density: 50 mA cm^{-2}) and (b) conditions (Ac: the acidic 0.5 M H_2SO_4, Neu: the neutral 1 M KPi, Alk: the alkaline 1 M KOH; RuO_x as the electrocatalyst for OER at 35 °C, current density: 300 mA cm^{-2}).

With the help of a more comprehensive model, especially fully considering the microscopic OER elementary reaction steps, macroscopic mass transport effect, electric double-layer effect, and all the possible degradation mechanisms, we believe that the DA method, with high information extraction capability, is prospective to identify and even quantify the dominant degradation mechanism. For example, after determining all the parameters at time *t* in the model by DA, we can analyse the partial derivative of the model with respect to *t* for each degradation mechanism. As a result, we will obtain a quantitative evaluation of the influence of each degradation mechanism on the overall degradation behaviour. By comparing the above results, we can finally confirm that the maximum absolute partial derivative corresponds to the dominant degradation mechanism. Moreover, this method identifies a dynamic dominant degradation mechanism that evolves with the degradation process because of the inclusion of time.

To make the above discussion clearer, we generalized our idea with a concise mathematical description below.

Assume that we have a comprehensive model and obtained all the model parameters by DA, and the degradation h_d can be expressed as:

$$h_d = h_d(\{g_i(t)\}) \quad \text{(eq. S33)}$$

where $g_i(t)$ is the i^{th} degradation mechanism related to time *t*, $\{g_i(t)\}$ is the set of all the degradation mechanisms.

For the influence on the overall degradation by the i^{th} degradation mechanism (here marked as $R_{d,i}(t)$), it can be expressed as:

$$R_{d,i}(t) = \frac{\partial h_d}{\partial g_i}\frac{\partial g_i}{\partial t} \quad \text{(eq. S34)}$$

We further define the normalized $R_{d,i}(t)$ as $r_{d,i}(t)$:

$$r_{d,i}(t) = \frac{R_{d,i}(t)}{\sum_i |R_{d,i}(t)|} \quad \text{(eq. S35)}$$

where $\sum_i |R_{d,i}(t)| > 0$. When $\sum_i |R_{d,i}(t)| = 0$, it indicates a stable state of the overall "degradation" at time *t*.

Inspired by *control function* (or *control factor*) and *degree of rate control* for quantifying the rate-determining step in chemical kinetics,[28, 29] here we suggest $r_{d,i}(t)$ as *degree of degradation control* of the i^{th} degradation mechanism. It is evident that the dominant degradation mechanism should have much larger $|r_{d,i}(t)|$ (like close to unity) than other

mechanisms. Similar to the discussion by Campbell,[29] we may set a threshold to quantify the above consideration, *e.g.*, the mechanism with $|r_{d,i}(t)| \in [0.6,1]$ can be regarded as the dominant degradation mechanism. In addition, apart from the above situation, when several mechanisms have relatively large and comparable $|r_{d,i}(t)|$, it means that these mechanisms jointly influence the degradation and we cannot ignore any of them. In such a case, we may regard them as codominant degradation mechanisms.

Broadly speaking, the term "degradation" used here may also include upgradation process, that is, the promotion of reaction performance. Under this circumstance, $r_{d,i}(t)$ may be called *degree of upgradation control*. To make it convenient, we recommend a more universal term "destabilization" rather than "degradation" or "upgradation". In this case, $r_{d,i}(t)$ can be nominated *degree of destabilization control* of the i^{th} destabilization mechanism. The related mechanism with the largest $|r_{d,i}(t)|$ (and much larger than others) can be regarded as the dominant destabilization mechanism. The model should be called destabilization model rather than degradation model.

Furthermore, if we set the increase in h_d as degradation and its decrease as upgradation, for the i^{th} destabilization mechanism, we can say that $r_{d,i}(t) > 0$ corresponds to a degradation trend, or $r_{d,i}(t) < 0$ indicates an upgradation trend, or $r_{d,i}(t) = 0$ shows a stable state of this mechanism at time *t*. From the time-dependant $r_{d,i}(t)$ we may expect a destabilization mechanism that has a dynamic degradation-upgradation process, *e.g.*, $r_{d,i}(t_1) > 0$ while $r_{d,i}(t_2) < 0$ to show a degradation-to-upgradation transition from t_1 to t_2 of the destabilization process.

References

(1) Amatore, C.; Jutand, A. Mechanistic and kinetic studies of palladium catalytic systems. *Journal of Organometallic Chemistry* **1999**, *576* (1), 254-278. DOI: 10.1016/S0022-328X(98)01063-8.

(2) Kozuch, S.; Shaik, S. A Combined Kinetic−Quantum Mechanical Model for Assessment of Catalytic Cycles: Application to Cross-Coupling and Heck Reactions. *Journal of the American Chemical Society* **2006**, *128* (10), 3355-3365. DOI: 10.1021/ja0559146.

(3) Kozuch, S.; Shaik, S. Kinetic-Quantum Chemical Model for Catalytic Cycles: The Haber−Bosch Process and the Effect of Reagent Concentration. *The Journal of Physical Chemistry A* **2008**, *112* (26), 6032-6041. DOI: 10.1021/jp8004772.

(4) Kozuch, S.; Shaik, S. How to Conceptualize Catalytic Cycles? The Energetic Span Model. *Accounts of Chemical Research* **2011**, *44* (2), 101-110. DOI: 10.1021/ar1000956.

(5) Kozuch, S. Steady State Kinetics of Any Catalytic Network: Graph Theory, the Energy Span Model, the Analogy between Catalysis and Electrical Circuits, and the Meaning of "Mechanism". *ACS Catalysis* **2015**, *5* (9), 5242-5255. DOI: 10.1021/acscatal.5b00694.

(6) Chen, J.; Chen, Y.; Li, P.; Wen, Z.; Chen, S. Energetic Span as a Rate-Determining Term for Electrocatalytic Volcanos. *ACS Catalysis* **2018**, *8* (11), 10590-10598. DOI: 10.1021/acscatal.8b03008.

(7) Wang, J. Controlling dynamic reconstruction chemistry for superior oxygen-evolving catalysts. *Chem* **2023**, *9* (7), 1645-1657. DOI: 10.1016/j.chempr.2023.06.001 (acccessed 2024/09/15).

(8) Zhu, X.; Huang, J.; Eikerling, M. Hierarchical Modeling of the Local Reaction Environment in Electrocatalysis. *Accounts of Chemical Research* **2024**, *57* (15), 2080-2092. DOI: 10.1021/acs.accounts.4c00234.

(9) Batchelor, T. A. A.; Pedersen, J. K.; Winther, S. H.; Castelli, I. E.; Jacobsen, K. W.; Rossmeisl, J. High-Entropy Alloys as a Discovery Platform for Electrocatalysis. *Joule* **2019**, *3* (3), 834-845. DOI: 10.1016/j.joule.2018.12.015 (acccessed 2024/09/15).

(10) Wittreich, G. R.; Alexopoulos, K.; Vlachos, D. G. Microkinetic Modeling of Surface Catalysis. In *Handbook of Materials Modeling: Applications: Current and Emerging Materials*, Andreoni, W., Yip, S. Eds.; Springer International Publishing, 2020; pp 1377-1404.

(11) Wang, M.; Kong, H.; Wang, J. Revisiting electrocatalytic oxygen evolution reaction microkinetics from a mathematical viewpoint. *Results in Chemistry* **2023**, *5*, 100985. DOI: 10.1016/j.rechem.2023.100985.

(12) Chen, F.-Y.; Wu, Z.-Y.; Adler, Z.; Wang, H. Stability challenges of electrocatalytic oxygen evolution reaction: From mechanistic understanding to reactor design. *Joule* **2021**, *5* (7), 1704-1731. DOI: 10.1016/j.joule.2021.05.005 (acccessed 2024/05/14).

(13) Du, K.; Zhang, L.; Shan, J.; Guo, J.; Mao, J.; Yang, C.-C.; Wang, C.-H.; Hu, Z.; Ling, T. Interface engineering breaks both stability and activity limits of RuO_2 for sustainable water oxidation. *Nature Communications* **2022**, *13* (1), 5448. DOI: 10.1038/s41467-022-33150-x.

(14) Risch, M. Upgrading the detection of electrocatalyst degradation during the oxygen evolution reaction. *Current Opinion in Electrochemistry* **2023**, *38*, 101247. DOI: 10.1016/j.coelec.2023.101247.

(15) Nicholson, D. Variation of surface area during the thermal decomposition of solids.

Transactions of the Faraday Society **1965**, *61* (0), 990-998, 10.1039/TF9656100990. DOI: 10.1039/TF9656100990.
(16) Hawa, T.; Zachariah, M. R. Coalescence kinetics of unequal sized nanoparticles. *Journal of Aerosol Science* **2006**, *37* (1), 1-15. DOI: https://doi.org/10.1016/j.jaerosci.2005.02.007.
(17) Shinagawa, T.; Ng, M. T.-K.; Takanabe, K. Electrolyte Engineering towards Efficient Water Splitting at Mild pH. *ChemSusChem* **2017**, *10* (21), 4155-4162. DOI: https://doi.org/10.1002/cssc.201701266.
(18) Wang, J. H. Self-Diffusion Coefficients of Water. *The Journal of Physical Chemistry* **1965**, *69* (12), 4412-4412. DOI: 10.1021/j100782a510.
(19) McCrory, C. C. L.; Jung, S.; Peters, J. C.; Jaramillo, T. F. Benchmarking Heterogeneous Electrocatalysts for the Oxygen Evolution Reaction. *Journal of the American Chemical Society* **2013**, *135* (45), 16977-16987. DOI: 10.1021/ja407115p.
(20) Wei, C.; Sun, S.; Mandler, D.; Wang, X.; Qiao, S. Z.; Xu, Z. J. Approaches for measuring the surface areas of metal oxide electrocatalysts for determining their intrinsic electrocatalytic activity. *Chemical Society Reviews* **2019**, *48* (9), 2518-2534, 10.1039/C8CS00848E. DOI: 10.1039/C8CS00848E.
(21) Trasatti, S.; Petrii, O. A. Real surface area measurements in electrochemistry. *Journal of Electroanalytical Chemistry* **1992**, *327* (1), 353-376. DOI: https://doi.org/10.1016/0022-0728(92)80162-W.
(22) Dam, A. P.; Papakonstantinou, G.; Sundmacher, K. On the role of microkinetic network structure in the interplay between oxygen evolution reaction and catalyst dissolution. *Scientific Reports* **2020**, *10* (1), 14140. DOI: 10.1038/s41598-020-69723-3.
(23) Binninger, T.; Mohamed, R.; Waltar, K.; Fabbri, E.; Levecque, P.; Kötz, R.; Schmidt, T. J. Thermodynamic explanation of the universal correlation between oxygen evolution activity and corrosion of oxide catalysts. *Scientific Reports* **2015**, *5* (1), 12167. DOI: 10.1038/srep12167.
(24) Cherevko, S. Stability and dissolution of electrocatalysts: Building the bridge between model and "real world" systems. *Current Opinion in Electrochemistry* **2018**, *8*, 118-125. DOI: 10.1016/j.coelec.2018.03.034.
(25) SciJinks, N. *How Reliable Are Weather Forecasts?* 2002. https://scijinks.gov/forecast-reliability (accessed 2024 Sept. 15th).
(26) Wang, J.; Guo, Y.; Wang, Y. A sequential random forest for short-term vessel speed prediction. *Ocean Engineering* **2022**, *248*, 110691. DOI: https://doi.org/10.1016/j.oceaneng.2022.110691.
(27) Armentrout, P. B.; Halle, L. F.; Beauchamp, J. L. Periodic trends in transition metal-hydrogen, metal-carbon, and metal-oxygen bond dissociation energies. Correlation with reactivity and electronic structure. *Journal of the American Chemical Society* **1981**, *103* (21), 6501-6502. DOI: 10.1021/ja00411a043.
(28) Laidler, K. J. Rate controlling step: A necessary or useful concept? *Journal of Chemical Education* **1988**, *65* (3), 250. DOI: 10.1021/ed065p250.
(29) Campbell, C. T. Future Directions and Industrial Perspectives Micro- and macro-kinetics: Their relationship in heterogeneous catalysis. *Topics in Catalysis* **1994**, *1* (3), 353-366. DOI: 10.1007/BF01492288.